Article

Discovery Medicine 2024; 36(181): 308–322
https://doi.org/10.24976/Discov.Med.202436181.29

Tube Formation Capability and Chemotaxis of Skin Pericytes

Yue Cui[1], Huang Lin[1,*], Yin-hua Zhao[1], Jia-xing Ma[1], Jia-xi Li[1]

[1]Department of Aesthetic Plastic Surgery and Laser Medicine, Beijing Anzhen Hospital, Capital Medical University, 100029 Beijing, China
*Correspondence: linhuang_72@mail.ccmu.edu.cn (Huang Lin)
Published: 20 February 2024

Background: Pericytes (PCs), the critical components of vessels, are implicated in wound repair. This study aimed to explore the roles of PCs in wound healing and angiogenesis.

Methods: Skin PCs and human dermal microvascular endothelial cells (HDMECs) were isolated from patients' upper eyelid skin. Immunofluorescence staining was used to characterize the morphology of PCs. Tube formation and transwell chemotaxis assays were performed to explore PC's tube-forming capability and chemotaxis. Finally, we investigated the effects of PCs and endothelial cells on wound repair using skin wound of a rat model.

Results: Skin PCs exhibited a double-protrusion structure and characteristic antigen expression of neural/glial antigen 2 (NG2)$^+$/platelet-derived growth factor receptor-β (PDGFR-β)$^+$/alpha-smooth muscle actin (α-SMA)$^+$/CD31$^-$. Skin PCs could directly form lumen-like structures in a two dimensional (2D) culture environment, and mild hypoxia and starvation promoted the lumen-like structure formation. Furthermore, skin PCs quickly formed more stable lumen-like structures than HDMECs in matrigel, and they recruited HDMECs in a three dimensional (3D) culture environment. Transwell chemotaxis assay showed that PCs and HDMECs were chemotactic to each other. PCs could develop lumen-like structures in the skin wounds of rat models. The number of PCs mounted in wounded skin was compared to normal skin. The ratio of PCs to endothelial cells gradually increased after skin injury and reached its maximum on the 3rd day.

Conclusions: Skin PCs have an excellent tube-forming capability and chemotaxis to endothelial cells. PCs might promote wound repair by recruiting endothelial cells.

Keywords: pericytes; wound repair; angiogenesis; tube formation assay; chemotaxis

Introduction

Pericytes (PCs), also known as mural or Rouget cells, are essential for wound angiogenesis [1,2]. These cells are found on the outer surface of the vasculature. They tightly wrap capillaries, arterioles, and venules [3], and hence regulate microvascular physiology, blood flow, and inflammatory cell trafficking [4]. Apart from promoting the stability and maturation of vessels, PCs can differentiate into stem cell-like progenitor cells [5]. Existing studies have confirmed the importance of skin PCs for tissue regeneration [6–8]. PCs aging is closely related to the capacity for skin regeneration [7,9].

Sprouting is the main mode of angiogenesis [10]. Tip and stalk cells form filamentous pseudopods, which create a lumen and proliferate to support bud elongation. The tip cells anastomose with cells of the neighboring buds to form a vascular ring [11]. PCs can stabilize new connections with endothelial cells, enhancing vessel maturation [12]. Disruption of PC recruitment by cytokines will lead to impaired angiogenesis [13]. Notably, PC coverage has an important impact on the development of diseases and wound healing [14]. Current research has shown that PCs are potential targets for skin regeneration, and numerous histological studies have tested their ability to promote skin regeneration [7,15]. The importance of PCs in wound healing is increasingly prominent [16–18]. Therefore, it is valuable to explore the role of PCs in wound healing.

However, a variety of problems limit the therapeutic application of PCs. For example, there are currently no specific markers and morphological features for PCs [19]. Therefore, investigating the properties of PCs will provide more avenues for identifying PCs.

Wound healing involves several complex processes, including immediate hemostasis, acute inflammation, proliferation, and maturation [20]. One of the key activities in the cell proliferation phase is angiogenesis which provides sufficient nutrition and oxygen to tissues while eliminating waste, thereby promoting tissue repair [21]. In addition, endothelial cells are important participants in the process of angiogenesis. To be specific, endothelial cells secrete matrix metalloproteinases (MMPs) to degrade the capillary basement membrane, and meanwhile, they proliferate and migrate outside of the original blood vessel to form new blood vessels [22]. This study aimed to explore the roles of

PCs in wound healing and angiogenesis. We examined the structure and function of skin PCs in two dimensional (2D) and three dimensional (3D) culture settings *in vitro*. Moreover, we explored the roles and changes of skin PCs during wound healing in a rat skin wound model. To our knowledge, this is the first study to demonstrate the tube-forming capability and the recruitment property of PCs. This study expands our understanding of skin PCs and the interaction between PCs and endothelial cells.

Materials and Methods

Cell Isolation and Culture

Upper eyelid skin tissues were obtained from 12 female patients (age of 18–35 years) who received blepharoplasty. This study was approved by the Ethics Committee of Anzhen Hospital (Approval number: 2023087x), and all patients signed informed consent forms. All procedures were conducted in accordance with the approved guidelines and the ethical requirements of the Helsinki Declaration. The skin tissues were processed to isolate PCs, human dermal microvascular endothelial cells (HDMECs), and fibroblasts (FBs). The isolated cells (PCs, HDMECs, and FBs) underwent a mycoplasma test using polymerase chain reaction (PCR) to confirm that they were not contaminated.

Isolation of Skin Pericytes (PCs)

PCs were obtained referred to the method described in a previous study [23]. Specifically, the skin flap was washed three times with phosphate-buffered saline (PBS) and cut into 0.5 $\times$ 0.5 $\times$ 0.1 cm sections. The sections were treated with the dispase II (2 mg/mL, #D4693, Sigma-Aldrich, Shanghai, China) to remove the epidermal layer from the dermis. The dermis was then digested with collagenase I (1.25 mg/mL, #1148089, Sigma-Aldrich, Shanghai, China) for 40 minutes to obtain the cell suspension containing PCs, and 2 mL of fetal bovine serum (FBS, #16140071, Gibco, Carlsbad, CA, USA) was added to terminate the reaction. Next, the skin flap was squeezed with plastic forceps, and the digested skin flap was filtered using a 40 µm filter. The filtered liquid was collected and centrifuged at 500 $\times$g for 5 minutes. After that, the cells were suspended in 2 mL pericyte medium (PM, #1201, Sciencell, Carlsbad, CA, USA) and incubated at 37 °C in a 5% CO_2 incubator. Considering the poor adherence of PCs, the cells growing on the culture flasks were washed with PBS, and those easily shed were collected. The collected cells were cultured in the PM that was changed every 3 days. After 7–9 days, the cells reached confluence, and were digested by trypsin and passaged. PCs with a high purity were obtained at the 3rd passage.

Isolation of Human Dermal Microvascular Endothelial Cells (HDMECs)

HDMECs were isolated in reference to the description of our previous study [24]. The pre-processing procedure for skin tissues was the same as the method for isolating PCs. The obtained cell suspension was sorted twice using magnetic beads containing CD31 (CD31 MicroBead Kit, #130-091-935, miltenyi biotec, Bergisch Gladbach, Germany) to obtain HDMECs. HDMECs were later cultured in endothelial cell medium (ECM; #1001, Sciencell, Carlsbad, CA, USA) with a density of 1×10^4 cells/cm^2, followed by an incubation at 37 °C in a 5% CO_2 incubator.

Isolation of Fibroblasts (FBs)

The isolation of FB was performed as previously described [25]. Dermal tissues were obtained from the patients and cut into 5 mm cubes using a scalpel. After that, the tissues were placed into a T75 flask. The flask was inverted for 2 hours to allow the tissues to adhere firmly. Next, the flask was turned upright, and added with 3 mL dulbecco's modified eagle medium (DMEM; #11965092, Gibco, CA, USA) containing 20% FBS. After one week, FBs began to extend out from the tissues. Another week later, the tissues were removed. FBs continued to be cultured until confluence. The cells were then digested using trypsin and passaged.

Cell Identification

The primary PCs were identified using flow cytometry and immunofluorescence staining. Neural/glial antigen 2 (NG2), alpha-smooth muscle actin (α-SMA), and platelet-derived growth factor receptor-β (PDGFR-β) have been considered the markers of primary PCs [26]. Flow cytometry was used to analyze NG2 positive staining and the purity of primary PCs, and immunofluorescence was used to observe the NG2, α-SMA, and PDGFR-β staining on PCs. Our previous research detected that HDMEC purity reached 95% after the cells were treated twice with magnetic beads containing CD31 [24]. In this study, we identified HDMECs only by observing the immunostaining of CD31, which was a marker of HDMECs [27]. FBs can express PDGFR-β and vimentin [28]. Therefore, we performed immunofluorescence staining of vimentin and PDGFR-β to identify FBs.

Construction of a Hypoxic Environment

We created a hypoxic environment to explore the tube-forming capability of PCs under hypoxia. Concretely speaking, cells were placed at 37 °C in a hypoxic chamber (90% N_2, 5% O_2, and 5% CO_2) for 2 hours.

Flow Cytometry

Flow cytometry was adopted for the identification of PCs. PCs (1×10^6) were incubated with 250 µL fixa-

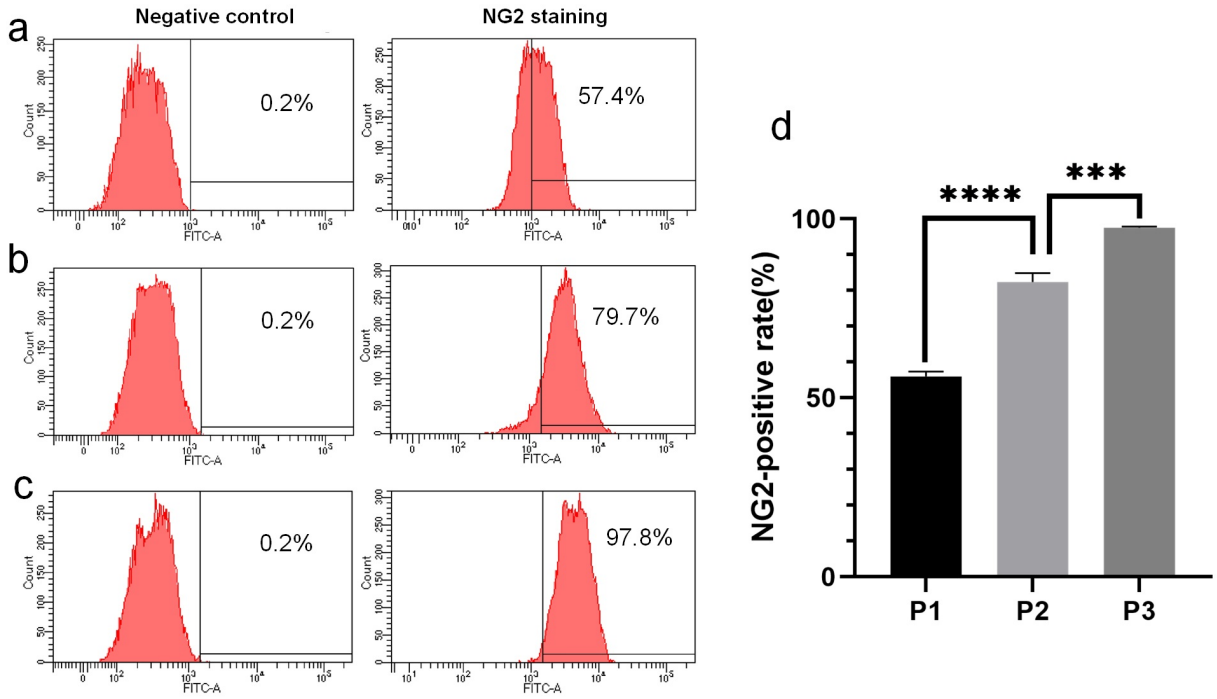

Fig. 1. The identification of skin pericytes (PCs). Flow cytometry was used to identify skin PCs. (a) Negative control and the percentage of cells with neural/glial antigen 2 (NG2)-positive staining reached 50% at passage 1. (b) Negative control and the percentage of cells with NG2-positive staining reached 80% at passage 2. (c) Negative control and the percentage of cells with NG2-positive staining reached 95% at passage 3. (d) NG2-positive rates in the first, second, and third passages were represented, respectively. ***$p < 0.001$, ****$p < 0.0001$.

tion/permeabilization solution (#554714, BD Biosciences, San Jose, CA, USA) in the dark for 20 minutes at 4 °C. Subsequently, the cells were washed twice with wash buffer (#554714, BD Biosciences, San Jose, CA, USA), and then added with 100 µL primary antibody NG2 (1:50, #55027-1-AP, Proteintech, USA) for a 30-minute incubation at 4 °C. After being washed twice, the cells were incubated with secondary Fluorescein Isothiocyanate (FITC) labeled antibody (1:200, #AS011, Abclonal, Wuhan, China) for 30 minutes at 4 °C. Following that, the cells were washed and resuspended. BD Biosciences LSR II flow cytometer (BD Biosciences, San Jose, CA, USA) and BD FACSDivaTM software (BD Biosciences, v8.0.1, San Jose, CA, USA) were applied to detect PCs. Data were analyzed using FlowJo v10.0.7 software (FlowJo, Ashland, OR, USA). Cells only added with the secondary antibody were set as negative controls.

Tube Formation Assay

Tube formation assay was adopted to evaluate the tube-forming capability of PCs in a 3D culture environment. The day before the assay, a matrigel (#354248, Corning, NY, USA) was placed at 4 °C to thaw the substrate gel. Meanwhile, a µ-Slide Angiogenesis (#81506, Ibidi, Munich, Germany) and pipette tips were cooled at 4 °C. Next, 10 µL of matrigel was added to the lower well of the µ-Slide Angiogenesis. The µ-Slide Angiogenesis was later placed in an incubator at 37 °C with 5% CO_2 for at least 30 minutes to allow matrigel polymerization. Subsequently, 50 µL of cell suspension (2×10^5 cells/mL) was added to each well. It was then incubated in the incubator at 37 °C with 5% CO_2, and tube formation in it was examined [29]. The branch point in tube formation assay was analyzed using the Angiogenesis analysis module in Image J v1.8.0 software (Media Cybernetics, Silver Spring, MD, USA).

The procedure for the co-forming tube assay was similar to the tube formation assay. After the matrigel was added into the lower well of the µ-Slide Angiogenesis, PCs or HDMECs were seeded individually into the matrigel. The cells were cultured before they adhered to the surface of the matrigel and not suspended. Next, another kind of cell (PCs or HDMECs) was inoculated into the matrigel for continued culture.

Animals

Twelve healthy male Sprague-Dawley rats weighing 250–300 g were purchased from Beijing Vital River Laboratory Animal Technology Co., Ltd. (Beijing, China). All rats were housed in a standard laboratory. Sodium pentobarbital at a dose of 30 mg/kg was injected into a peripheral ear vein for anesthesia. To construct a skin wound of rat

model, 4 circular wounds of 6 mm diameter were created on the abdominal area of all rats using a biopsy punch. The wounds were covered with Omiderm (Omikron Scientific Ltd., Rehovot, Israel). All rats showed no significant infection, and the regenerated tissues were collected on day 1, day 3, day 5, and day 7, respectively. Meanwhile, normal skin was collected from all rats. Normal skin refers to skin tissues without wounds prior to sampling. All animal experiments were approved by Ethics Committee of Institute of Zoology Chinese Academy of Science (approval ID: IOZ-IACUC-2023-007), and they also complied with the approved ethical guidelines. Specialized surgeons performed all surgeries, and all efforts were made to minimize the distress of the animals.

Immunofluorescence Staining

Cells were inoculated onto 24-well plates containing coverslips. After 1–2 days of cultivation, the coverslips were washed 3 times with PBS and fixed in 4% paraformaldehyde (#G1101, Servicebio, Wuhan, China) for 20 minutes at 25 °C. The cells were permeabilized using 0.3% Triton X-100 (#T8200, Solarbio, Beijing, China) for 10 minutes and incubated with 5% bovine serum albumin (BSA, #A8010, Solarbio, Beijing, China) for 1 hour. Following that, the cells on coverslips were incubated for 24 hours at 4 °C with primary antibodies. The primary antibodies included NG2 (#A3592, Abclonal, Wuhan, China), PDGFR-β (#A19531, Abclonal, Wuhan, China), CD31 (#GB12064, Servicebio, Wuhan, China), vimentin (#GB111308, Servicebio, Wuhan, China) and α-SMA (#GB13044, Servicebio, Wuhan, China). The dilution of the antibodies was 1:100. Again, the cells were washed with PBS for 15 minutes at room temperature and then conjugated with secondary antibodies (FITC or Cy3; 1:500 dilution) for 1 hour. Finally, 10 µL anti-fluorescence quenching mounting medium containing 2-(4-Amidinophenyl)-6-indolecarbamidine dihydrochloride (DAPI) (#p36966, Thermofisher, CA, USA) was added to the cells.

The skin tissues were extracted from the rats. The epidermis of the skin was removed, while the dermal tissues were retained. The dermal tissues were initially fixed in 4% paraformaldehyde (#G1101, Servicebio, Wuhan, China) and subsequently embedded in paraffin. Thin sections with a thickness of 5 µm were obtained using a microtome. Tris-EDTA (#G1203, Servicebio, Wuhan, China) was used for the antigen retrieval on paraffin sections. Blocking was accomplished by incubating the sections with 5% BSA (#A8010, Solarbio, Beijing, China) to minimize nonspecific antibody binding. Next, the sections were incubated with primary antibodies for 24 hours at 4 °C, followed by another incubation with corresponding fluorescent secondary antibodies. Finally, fluorescence signals on the sections or cells were visualized using the Eclipse TE2000-s fluorescent microscope (Nikon, Melville, NY, USA), and image acquisition and analysis were conducted accordingly by NIS-Elements BR Analysis software (v5.20.00, Nikon, Melville, NY, USA).

Transwell Chemotaxis Assay

Transwell assay was performed referring to a previous study [30]. A transwell with membrane pores of 8 µm diameter (#3464, Corning, NY, USA) and cell suspensions (5×10^5 cells/mL) were prepared. The upper chamber of the transwell was introduced with 200 µL cell suspensions (1×10^5 cells), and the lower chamber with 600 µL of culture medium or medium containing cells. The cells were cultured for 48 hours at 37 °C in a 5% CO_2 incubator. Cotton swabs were used to wipe off the cells remaining on the upper surface of the upper chamber. The cells in the lower side of the upper chamber were fixed with 4% paraformaldehyde and then stained with 0.1% hematoxylin solution (#H8070, Solarbio, Beijing, China) for 20 minutes. Five visual fields were randomly examined and counted.

Statistical Analysis

Each experiment was conducted at least three times (technical replicates). Data were presented as the mean $\pm$ standard deviation (SD). Statistical analysis was done using GraphPad Prism v9.0 (GraphPad Software Inc., La Jolla, CA, USA). Analyses were conducted by one-way analysis of variance (ANOVA) or Student's *t*-test. The data among groups at different time points were compared by repeated-measures ANOVA. $p \leq 0.05$ was considered statistically significant.

Results

Morphological Characterization and Identification of Skin Pericytes

First, we observed and identified the primary skin PCs. Flow cytometry was used to analyze the purity of primary skin PCs. The results showed that PCs were identified by NG2-positive staining (Fig. 1), and the percentage of NG2-positively stained PCs reached 95% at passage 3 (Fig. 1c), and that high-purity PCs were successfully obtained.

We subsequently identified PCs, HDMECs, and FBs using immunofluorescence. It was observed that PCs expressed NG2, α-SMA, and PDGFR-β (Fig. 2a–d,i–l), which were the primary markers of PCs. Moreover, PCs showed CD31-negative staining (Fig. 2a–d). The proportion of PCs expressing $NG2^+/CD3^-$ was more than 95% (Fig. 2a–d). Collectively, skin PCs mainly expressed $NG2^+$/PDGFR-β^+/α-$SMA^+/CD31^-$. CD31 is a specific marker of HDMECs. HDMECs exhibited CD31-positive staining (Fig. 2e–h). FBs displayed the PDGFR-β and vimentin-positive staining (Fig. 2m–p, **Supplementary Fig. 1**).

Because different cells have different markers, we distinguished PCs from HDMECs and FBs by double staining. CD31 and NG2 double staining was used to distinguish PCs

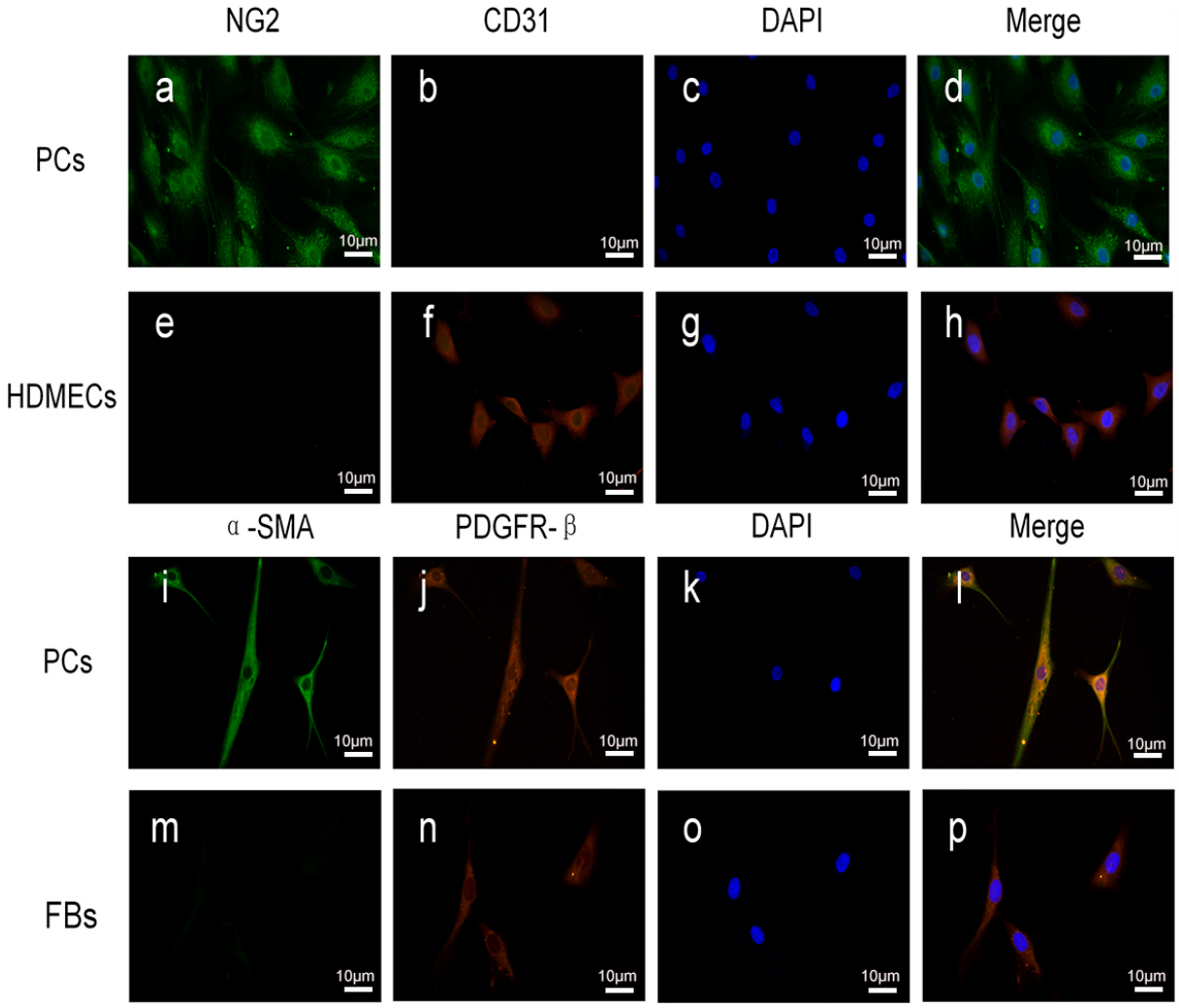

Fig. 2. Skin PCs specifically express NG2$^+$/platelet-derived growth factor receptor-β (PDGFR-β)$^+$/alpha-smooth muscle actin (α-SMA)$^+$/CD31$^-$. (a–h), Immunofluorescence staining was adopted to detect the expression of CD31 (red) and NG2 (green) in PCs (a–d) and human dermal microvascular endothelial cells (HDMECs) (e–h). Nuclei were stained with 2-(4-Amidinophenyl)-6-indolecarbamidine dihydrochloride (DAPI) (blue). Scale bar = 10 µm. (i–p) The expression levels of α-SMA (green) and PDGFR-β (red) in PCs (i–l) and fibroblasts (FBs) (m–p) were also detected by immunofluorescence staining. Nuclei were stained with DAPI (blue). Scale bar = 10 µm.

(NG2$^+$/CD31$^-$) from HDMECs (NG2$^-$/CD31$^+$) (Fig. 2a–h). The results of PDGFR-β and α-SMA double staining showed that PCs expressed PDGFR-β^+/α-SMA$^+$, while FBs expressed PDGFR-β^+/α-SMA$^-$ (Fig. 2i–p). Overall, we identified and distinguished FBs, PCs, and HDMECs.

Then, we observed the morphological characterization of skin PCs. Skin PCs exhibited a double cell protrusion shape (Fig. 3a,b). Due to the elongated cell protrusion on both sides, the length of skin PCs reached 80 µm. The length of cell protrusion on one side of some PCs reached 50 µm (Fig. 3b), and the whole cell length was 100 µm. When PCs were cultured in the matrigel, we could observe a cell protrusion (Fig. 3c). Compared with PCs, HDMECs have a shorter diameter of about 10–15 µm [31]. We observed under a microscope that one PC was wrapped around multiple HDMECs (Fig. 3d). A similar phenomenon was also found when PCs and HDMECs were cultured together in the matrix (Fig. 3e).

The Tube-Forming Capability of Skin Pericytes in a 2D Culture Environment

Next, we observed the tube-forming capability of different types of cells in a 2D culture environment. The 2D culture environment is defined as direct inoculation in culture flasks. We found that HDMECs appeared cobblestone-like rather than lumen-like structures in *in vitro* culture (Fig. 4a–c). The PCs did not form obvious lumen-like structures on the first day (Fig. 4d). After 3 days of cultivation,

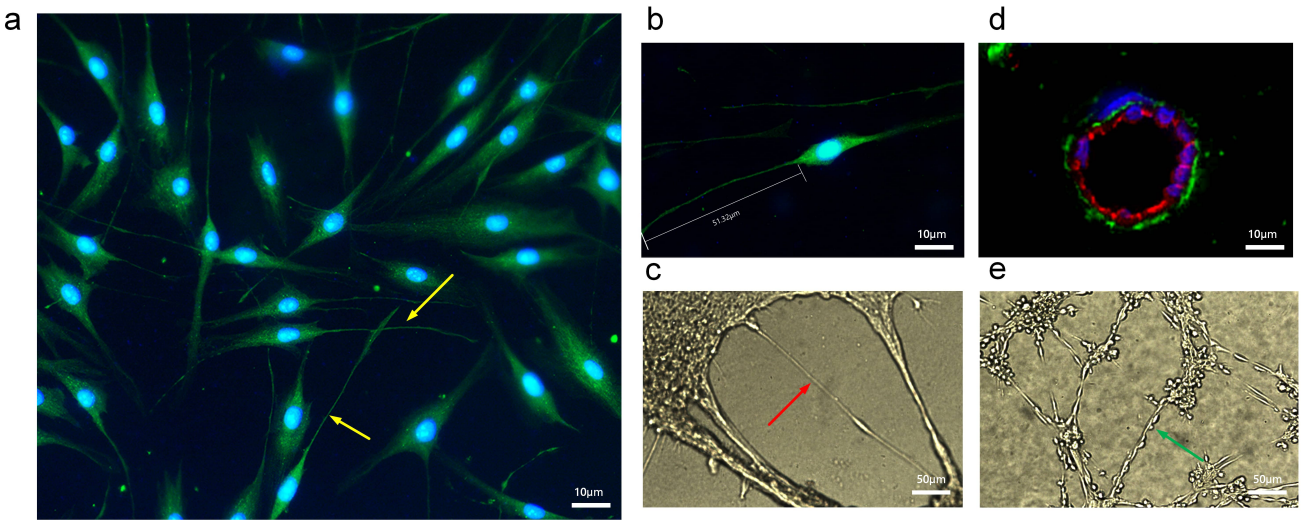

Fig. 3. Skin PCs exhibit a double protrusion structure. (a) The double cell protrusion shape of skin PCs (yellow arrows) was observed using immunofluorescence staining. Scale bar = 10 μm. (b) The cell protrusion on the one side of the skin PCs was up to 50 μm. Scale bar = 10 μm. (c) The cell protrusion of skin PCs (red arrow) was observed after being cultured in the matrigel. (d) One skin PC (green) was wrapped around multiple HDMECs (red) under immunofluorescence staining. The nucleus displayed blue fluorescence. Scale bar = 10 μm. (e) The matrigel distribution of PCs and HDMECs was observed after culturing PCs and HDMECs together in a matrix. The green arrow represents that PCs were wrapped around multiple HDMECs.

PCs formed a distinct lumen-like structure (Fig. 4e). However, the lumen-like structure of PCs struggled to maintain due to high density after 5 days of cultivation (Fig. 4f). FBs, with a morphology similar to that of PCs, were evenly arranged and grew in a spiral pattern (Fig. 4g–i). Even on day 5, FBs could not sustain a lumen-like structure; instead, they proliferated all over the bottom of the flask (Fig. 4i).

However, not all primary PCs showed good tube-forming capability in the 2D culture environment (Fig. 5a). This may be attributed to PCs' rapid proliferation or quiescent state, making it difficult to observe the lumen-like structure. It has been reported that PCs exist in one of two states – quiescent or active – each with a characteristic cell shape and structure [28]. An improved tube-forming capacity of PCs could be achieved through specific induction methods. In our study, we compared the tube-forming capability of PCs from 12 patients in the 2D environment. As a result, the PCs isolated from 5 patients (40%) found it difficult to form lumen-like structures without induction.

We found that starvation and mild hypoxia could promote the tube-forming capability of PCs. In this study, we cultured skin PCs in PM with 0.2% pericyte growth factor (PGF) and 1% FBS. Due to the lack of nutrients, the excessive proliferation of PCs was inhibited. Meanwhile, PCs formed pronounced lumen-like structures (Fig. 5b). We also investigated the tube-forming capability of PCs under mild hypoxia. The results showed that the mild hypoxic condition did not significantly reduce the number of PCs but enhanced their tube-forming capacity (Fig. 5c). It suggested that hypoxia enhanced their tube-forming capability. In addition, when PCs were cultured under both mild hypoxia and starvation, many small lumen-like structures were formed, and the number of PCs was not reduced (Fig. 5d). Overall, mild hypoxia and starvation improved the efficiency of lumen-like structure formation in PCs.

Furthermore, the effects of cell passage on the tube-forming capability of primary skin PCs were assessed. Notably, the lumen-like structure of PCs was most apparent in the 4th–7th generation. After the 9th generation, the PCs had difficulty forming stable and continuous lumen-like structures (Fig. 5e). The tube-forming capability of PCs gradually decreased with the increase of cell passage times. Through immunofluorescence staining, the tube-forming structure of PCs could be clearly observed in 2D (Fig. 5f). In short, PCs could form a distinct lumen-like structure in the 2D culture environment, and mild hypoxia and starvation promoted the formation of lumen-like structures. It was evident that the viability and status of PCs influenced the tube-forming capability.

The Tube-Forming Capability of Skin Pericytes in a 3D Cultivation Environment

We further investigated the tube-forming capability of skin PCs in a 3D culture environment. PCs formed apparent lumen-like structures with intact walls and clear lumens within 1 hour after the addition of the cell suspensions to the matrigel (Fig. 6a). The lumen structures remained unchanged after 4 hours of incubation (Fig. 6b). However, the lumen-like structures formed by PCs began to degrade at 8 hours (Fig. 6c). At 16 hours, most of the lumen-like structures were degraded (Fig. 6d), and PCs hardly maintained their morphology at 24 hours (Fig. 6e). In terms of quanti-

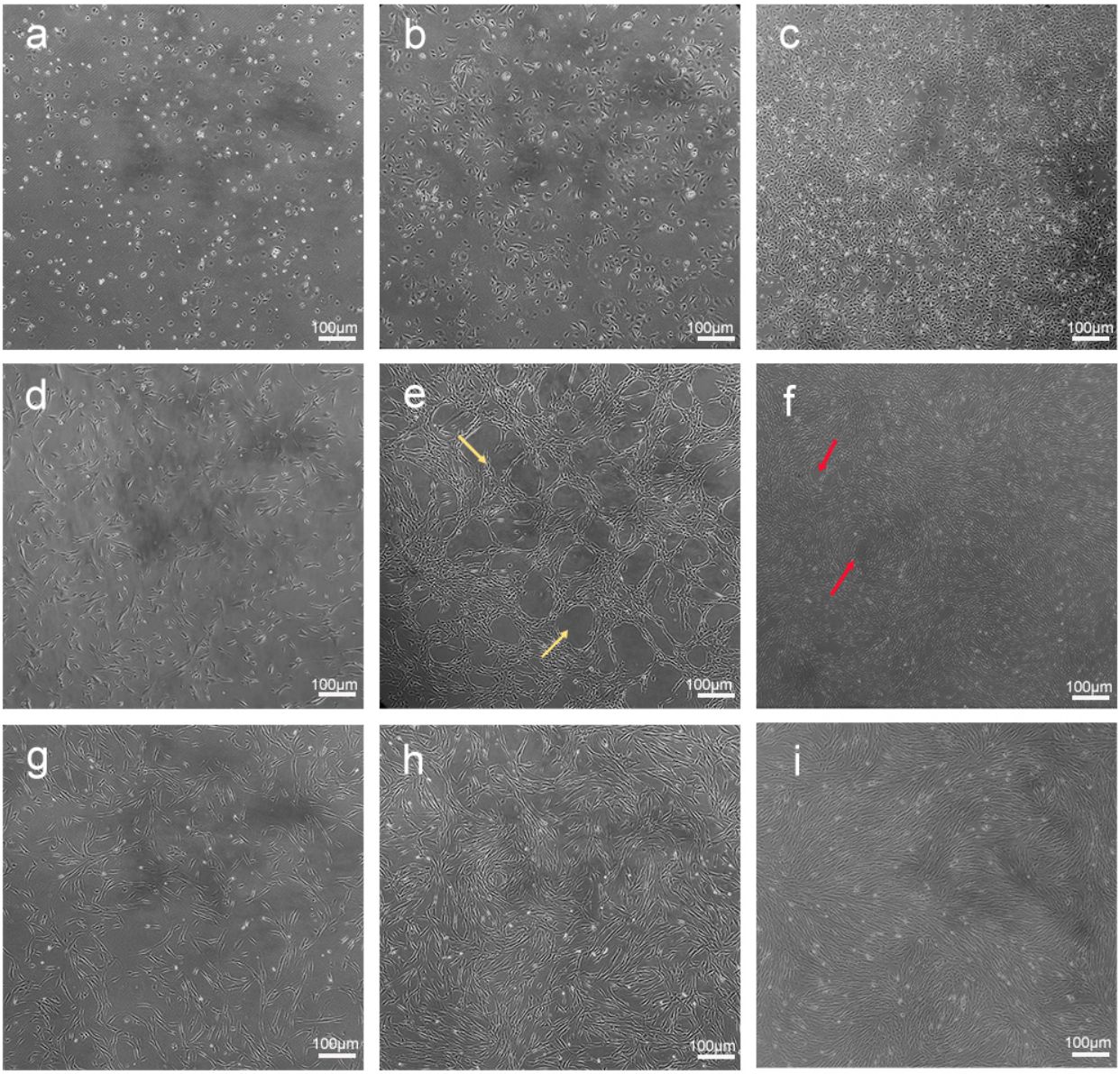

Fig. 4. PCs form lumen-like structures in a two dimensional (2D) culture environment. (a–c) The morphology of HDMECs cultured for 3 days in the 2D culture environment. (d–f) The morphology of PCs after the incubation for 1 (d), 3 (e), and 5 (f) days in the 2D culture environment. Yellow arrows represent lumen-like structures; red arrows represent the degradation of lumen-like structures. (g–i) The morphology of FBs cultured for 1 (g), 3 (h), and 5 (i) days in the 2D culture environment. Scale bar = 100 μm.

tative analysis results, the number of branch points was significantly reduced after 4 hours of culture in the PCs group (Fig. 6p).

In comparison with PCs, the rate of tube formation was slower in HDMECs. At 1 h, HDMECs did not form the luminal structure (Fig. 6f). HDMECs started to form intermittent lumen-like networks at 4 hours (Fig. 6g), and a better lumen formation was achieved at 8 hours (Fig. 6h). Compared to the lumen-like structure of skin PCs, the integrity of the tubular wall formed by HDMECs was poorer, and the lumen morphology was slightly worse (Fig. 6h). At 16 h, the lumen structure of HDMECs was degraded (Fig. 6i). At 24 h, the lumen structure could not be seen (Fig. 6j). The number of branch points in HDMECs was lower than that in PCs at 1 hour, increased significantly at 8 hours, and rapidly decreased at 16 and 24 hours (Fig. 6p).

The above results indicated that it was difficult for a single type of cell to maintain lumen-like structures for more than 24 hours. Therefore, we speculated that mixed cells can prolong the maintenance time of the lumen-like structure. When the PCs and HDMECs were mixed, the tube-forming time was shorter than that in HDMECs alone but not as short as that for PCs alone. At 1 hour, the mixed cells formed the lumen-like structure (Fig. 6k), and the structure could be observed at the 4h, 8 h and 16 h (Fig. 6l–n). Even at 24 hours, the lumen-like structure was not de-

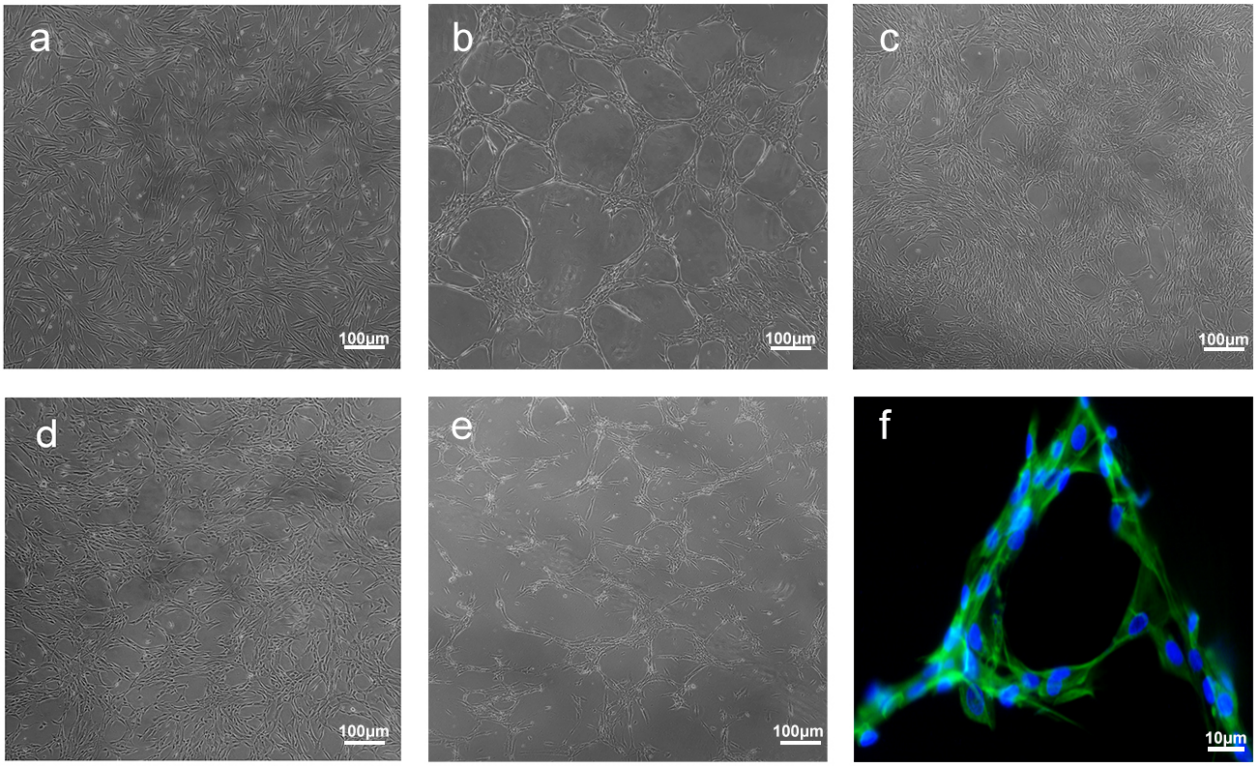

Fig. 5. Starvation and mild hypoxia promote the tube-forming capability of PCs in a 2D culture environment. (a) Some PCs routinely cultured in the 2D environment did not form obvious lumen-like structures. Scale bar = 100 μm. (b) The large-diameter lumen-like structures of PCs were formed under starvation conditions. Scale bar = 100 μm. (c) PCs formed lumen-like structures under mild hypoxic conditions. Scale bar = 100 μm. (d) PCs formed numerous small lumen-like structures under mild hypoxia and starvation conditions. Scale bar = 100 μm. (e) PCs had difficulty forming stable and continuous lumen-like structures after the 9th generation. Scale bar = 100 μm. (f) The lumen-like structures of PCs were observed by immunofluorescence staining. Scale bar = 10 μm.

graded (Fig. 6o). We observed that the number of branch points in the mixed group at 1 hour was lower than in the PCs group but higher than in the HDMECs group. Subsequently, the number of branch points in the mix group decreased at 8 hours (Fig. 6p). Our results suggested that a mixture of skin PCs and HDMECs could prolong the maintenance time of lumen-like structures.

FBs could aggregate into clusters directly in the matrigel (Fig. 6q). Some of the active FBs formed dendritic structures but could not form lumen-like structures (Fig. 6r). At 24 hours after incubation, the FBs still had no obvious lumen-like structures. In contrast, PCs formed many lumen-like structures with intact and uniform walls (Fig. 6s).

Mutual Chemotaxis of Skin Pericytes and Endothelial Cells

The transwell assay explored the interactions between HDMECs and PCs. We designed multiple groups for the transwell assay (Fig. 7a). When cells in the lower chamber were chemotactic to cells in the upper chamber, the cells in the upper chamber could pass through the membrane to the lower side of the upper chamber (Fig. 7a). To analyze the cell chemotaxis, we observed and counted the cells in the lower side of the upper chamber. The results are displayed in Fig. 7b–h.

First, HDMECs were introduced into the upper chamber, and PCs or PM (no cell) into the lower chamber (Fig. 7b,c). Compared to PM, the cell number was higher in the lower chamber with PCs ($p < 0.05$, Fig. 7h). It suggested that PCs in the lower chamber could recruit more HDMECs than PM without PCs. Similarly, we placed the PCs in the upper chamber and HDMECs or ECM (no cell) in the lower chamber (Fig. 7d,e). The cell number was higher in the HDMECs group than in the ECM group ($p < 0.05$, Fig. 7h). This indicated that HDMECs also recruited PCs. Finally, the upper chamber was added with HDMECs, and the lower chamber with FBs or DMEM (no cell) (Fig. 7f,g). Consequently, there was no significant difference between the two groups (Fig. 7h). In summary, PCs and HDMECs were chemotactic to each other.

The co-forming tube assay examined the mutual chemotaxis of these two types of cells. PCs and endothelial cells were added to the matrigel in a different order: (1) PCs-HDMECs: PCs were added first, and then HDMECs were added for co-culture with PCs; (2) HDMECs-

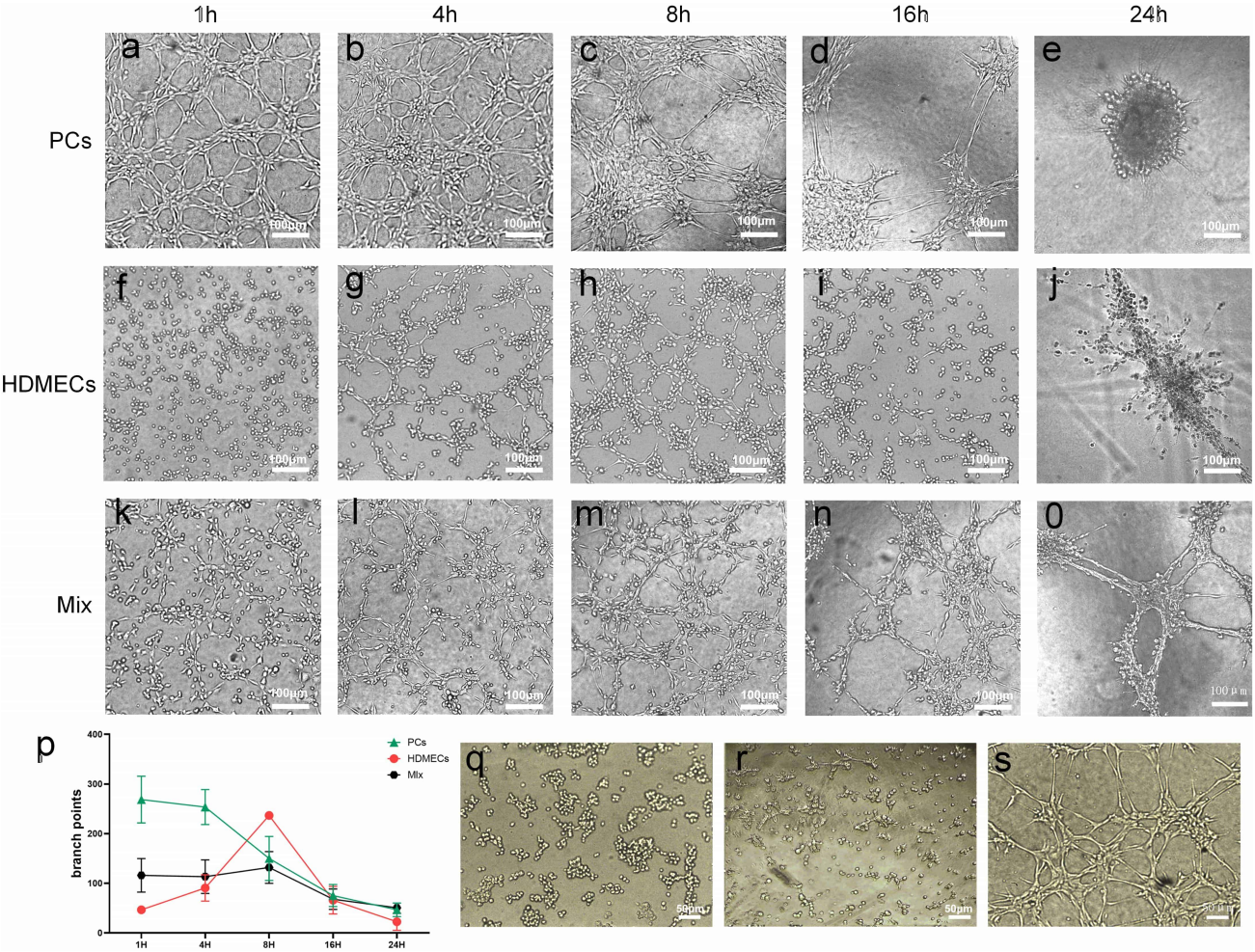

Fig. 6. Skin PCs form lumen-like structures in a three dimensional (3D) culture environment. (a–p) The tube-forming capability of PCs (a–e), HDMECs (f–j), and their mixed cells (k–o) was assessed by tube formation assay. Cells were observed after 1 h, 4 h, 8 h, 16 h, and 24 h of culture. Scale bar = 100 µm. The branch points in the tube formation assay were subjected to quantitative analysis (p), n = 3. (q–s) The tube-forming capability of FBs (q,r) and PCs (s) was detected by tube formation assay. Some FBs were aggregated into clusters (q) or formed dendritic structures (r) in matrigel, while PCs formed lumen-like structures (s) in matrigel. Scale bar = 50 µm.

PCs: HDMECs were added first, and then PCs followed. First, the PCs (Fig. 7i) or HDMECs (Fig. 7l) were individually seeded in matrigel. Next, another cell type (PCs or HDMECs) was added into the matrigel. We found that the cells added later to the matrigel were initially randomly distributed (Fig. 7j,m). These cells were later gradually attracted to the location of the cells previously cultured in the matrigel. Eventually, there were almost no discrete cells (Fig. 7k,n). It was clear that PCs and endothelial cells also recruited each other in the co-forming tube assay.

We directly examined the chemotaxis of PCs to HDMECs in the matrigel. The following two groups were set: (1) In the experimental group, PCs were first inoculated in the matrigel, followed by HDMECs; (2) In the control group, HDMECs were directly added in the matrigel. HDMECs floated uniformly at first in the experimental group. Subsequently, HDMECs were recruited and accumulated near PCs (Fig. 7o–t). In contrast, HDMECs in the control group remained uniformly discrete during this period, and no aggregation or attraction occurred, the cell morphology remained stable without significant changes at 15 and 20 min (Fig. 7u–z). Briefly speaking, PCs could recruit HDMECs in a 3D culture environment.

Functions and Changes of Skin Pericytes in Angiogenesis

We established skin wounds of rat models to assess the capacity of skin PCs *in vivo*. Complete lumen-like structures are crucial for wound repair. We discovered that neovascularization covered by PCs had good morphology and could develop lumen-like structures (Fig. 8a). However, the tissues only containing endothelial cells (without PCs) failed to form the lumen-like structures (Fig. 8b). Additionally, endothelial cells partially encapsulated by PCs formed part of the lumen (Fig. 8c). The different lumen types described above were often simultaneously present in skin

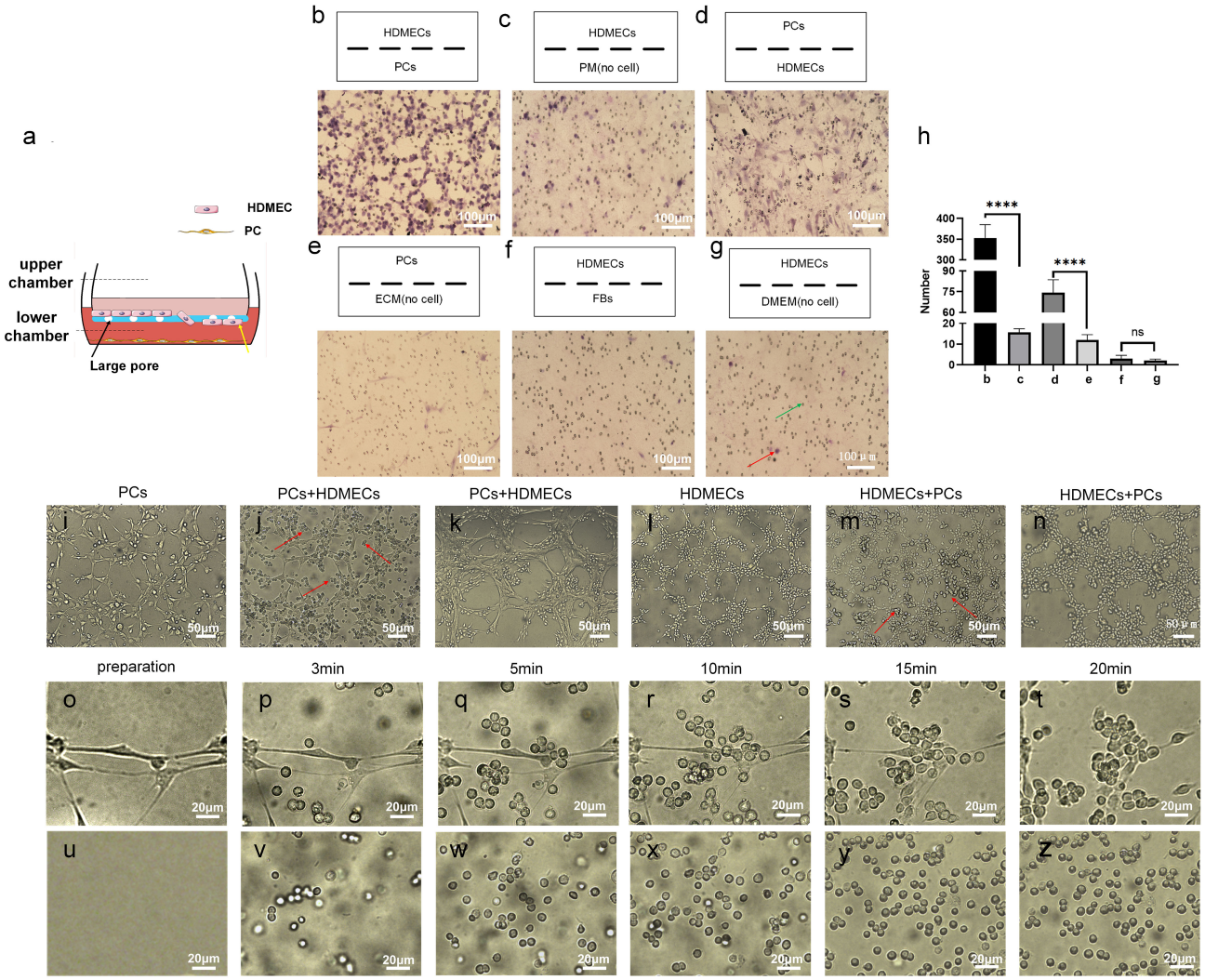

Fig. 7. PCs recruit HDMECs in a 3D cultivation environment. (a–h) The chemotaxis between HDMECs and PCs was explored by transwell assay. The design diagram of transwell assay (a), the grouping design and results (b–g), and the quantitative analysis of transwell (h) were displayed. Yellow arrow indicates the cells passing through the membrane (a); the red arrow represents the HDMECs passing through the membrane (g), and the green arrow represents the pores on the membrane (g). Scale bar = 100 μm. In (h), the group names represent the corresponding numbers in the transwell result images, ****$p < 0.0001$, and ns indicates no significant difference. N = 3. (i–n) The co-forming tube assay examined the mutual chemotaxis between PCs and HDMECs. (i–k) PCs-HDMECs: PCs were cultured alone in matrigel (i), and then HDMECs were added into the matrigel and co-cultured with PCs (j,k); (l–n) HDMECs-PCs: HDMECs were seeded to matrigel first alone (l), and PCs were next added for co-culture (m,n). Red arrows indicate independent cells. Scale bar = 50 μm. (o–z) The chemotaxis of PC to HDMECs was evaluated in the matrigel. In the experimental group (o–t), PCs were first inoculated in the matrigel, and HDMECs were subsequently added. In the control group (u–z), HDMECs were directly added to the matrigel. Scale bar = 20 μm.

wounds (Fig. 8d). We also observed lumen-like structures on the trauma surface, primarily with PCs and a few endothelial cells on their inner side (Fig. 8e). This may be a lumen formed by scattered PCs. From the above description, PCs were important for the formation of lumen-like structures during the repair of skin wounds. Furthermore, we speculated that controlling the ratio of PCs to endothelial cells might promote the formation of lumen-like structures.

To verify this hypothesis, the pericyte/endothelial cell ratio was analyzed in a rat skin wound model by calculating the green/red immunofluorescence area ratio. The proportion of PCs was significantly lower in the normal skin dermis, and PCs encapsulated only a few vessels (Fig. 9a). During trauma healing, however, we found a noticeable increase in the number of green fluorescent NG2 staining-labeled PCs (Fig. 9b–f). On the first day of wound healing, the number of PCs significantly increased, but it was

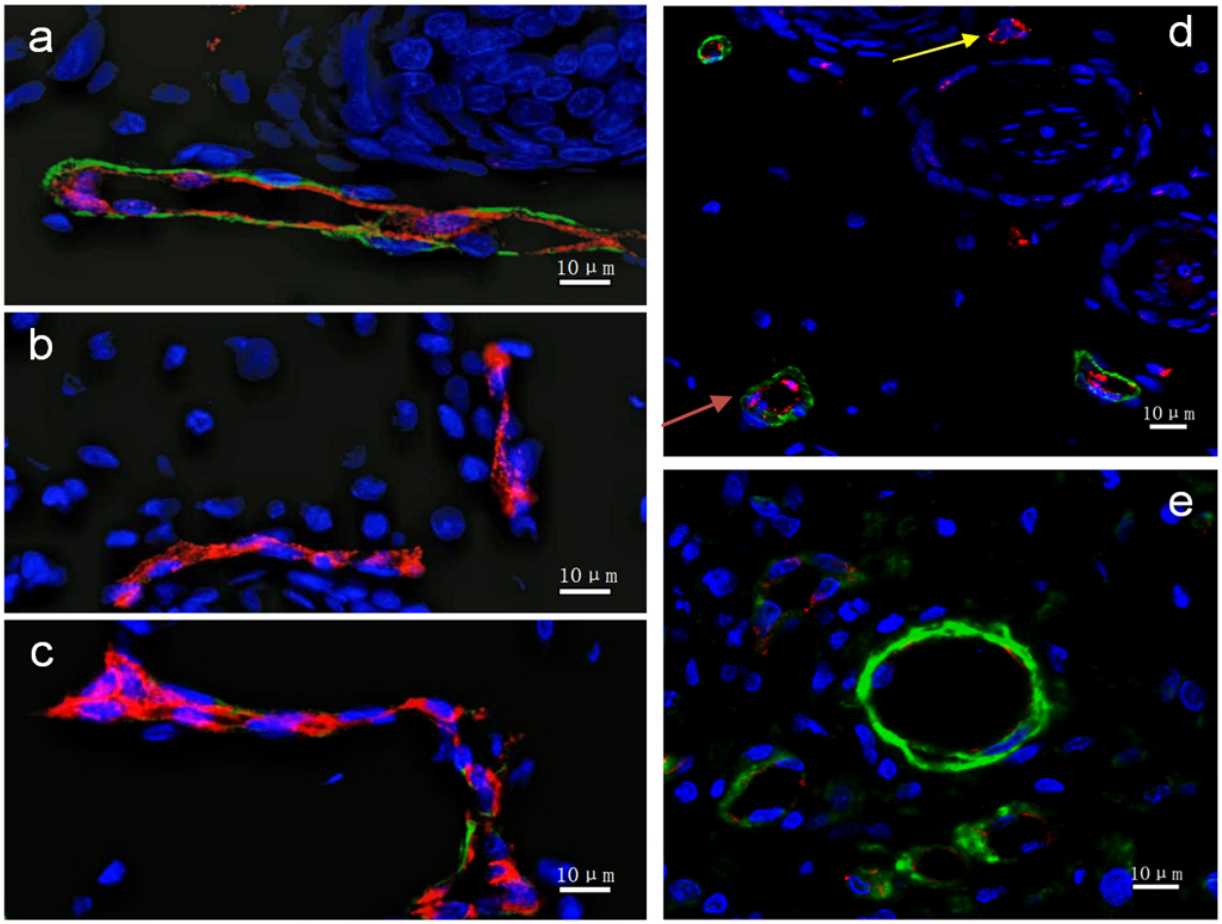

Fig. 8. Skin PCs maintain the formation of neovascular lumens during the skin wound repair in rats. (a–e) Immunofluorescence staining observed the tissue structure and cell type in skin wounds. PCs, endothelial cells, and cell nuclei were stained with NG2 (Green), CD31 (Red), and DAPI (Blue), respectively. Scale bar = 10 μm. (a) Functional vessels completely encapsulated by PCs easily formed lumen-like structures. (b) Non-functional vessels only containing endothelial cells failed to create lumen-like structures. (c) Neovascularization containing endothelial cells and PCs formed part of the lumen. (d) Multiple types of vessels existed in skin wounds at the same time. The yellow arrow indicates the luminal structure formed only by HDMECs. The red arrow indicates the luminal structure formed by the combination of PCs and HDMECs. (e) PCs-dominated lumen-like structures comprised primarily PCs and a few endothelial cells on their inner side.

difficult to help the vessels form stable lumen-like structures (Fig. 9b). On day 3, many blood vessels wrapped by PCs formed stable lumen structures (Fig. 9c). Besides, the pericyte/endothelial cells ratio peaked at seven times that of normal skin. On day 5, the pericyte/endothelial cell ratio began to decrease (Fig. 9d) and appeared to increase on day 7 (Fig. 9e). Fig. 9f showed the statistics of immunofluorescence area change of pericyte/endothelial cells. The above results revealed that the number of PCs significantly increased during wound healing. Nevertheless, the change fluctuated, resulting in the formation of well-structured neovascularization encapsulated by PCs. In Fig. 9g, the left side of the white line showed the regenerated tissue vascular staining of the wound, while the right side of the white line showed normal skin staining. In addition, we observed an increased number of PCs in healing skin.

Discussion

Wound angiogenesis is a complex physiological and pathological process. However, the role of PCs in wound angiogenesis is still unclear, and in-depth research is lacking. This study looked at the role of skin PCs in angiogenesis during wound healing from the perspectives of their morphology, function, and chemotaxis.

PCs are tissue-specific in terms of both morphology and function. Existing research on PCs has focused on the nervous system and the retina [32,33]. The blood-brain barrier or blood-retinal barrier shows a 1:1 PC/endothelial cell ratio [34]. The presence of PCs is vital to the normal function of the barriers [35,36]. In contrast, the pericyte/endothelial cell ratio in human lungs and skin is estimated to be 1:10 [37]. The α-SMA expression in cerebral vasculature is unstable and often difficult to detect [38]. In

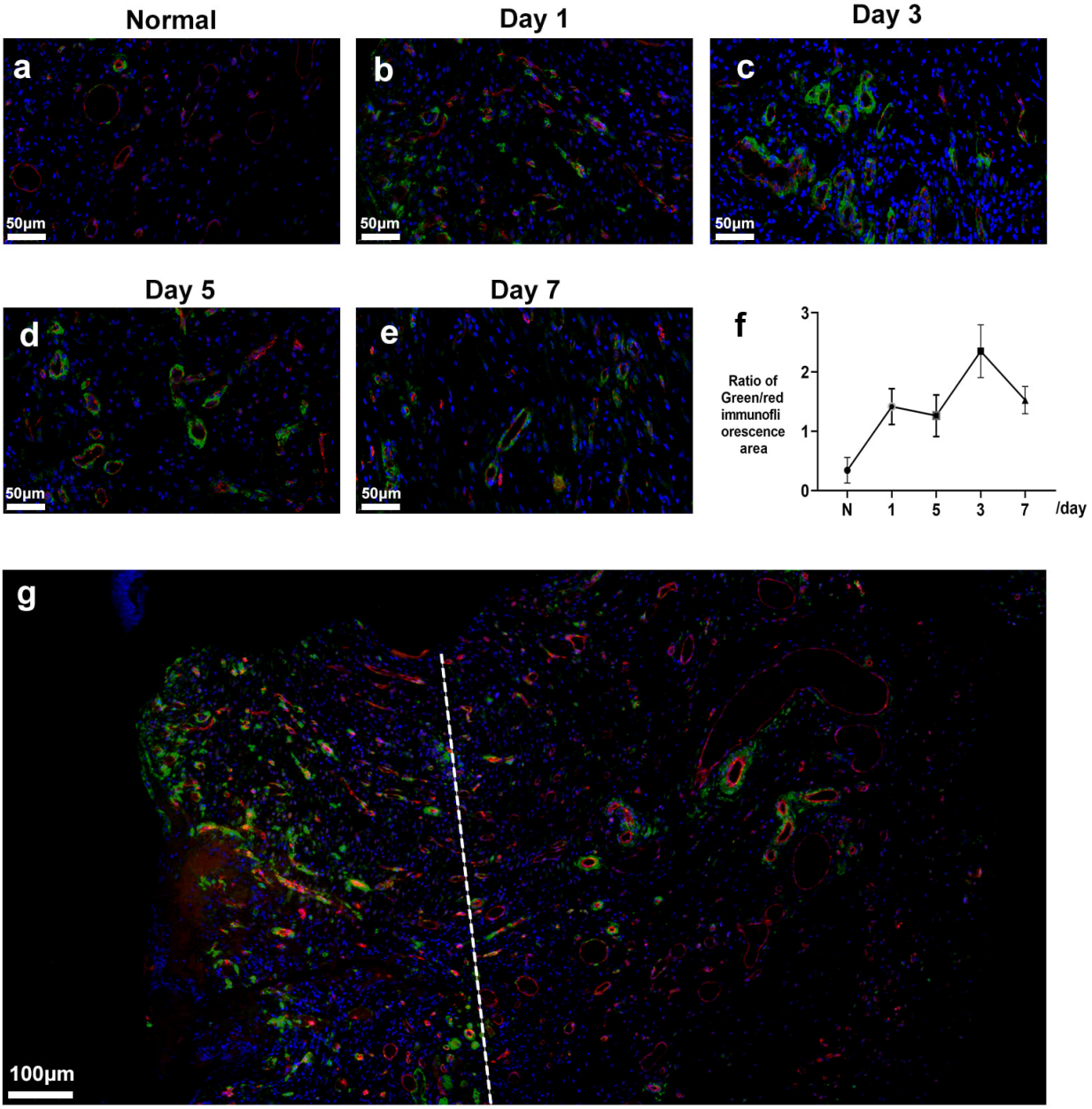

Fig. 9. The balance of the pericyte/endothelial cell ratio promotes wound repair in rats. (a–e) Immunofluorescence staining was adopted to observe PCs and endothelial cells in normal skin and wound tissues. PCs, endothelial cells, and cell nuclei were stained with NG2 (green), CD31 (red), and DAPI (blue), respectively. Scale bar = 50 μm. (a) The vasculature of normal skin consisted mainly of endothelial cells and a small number of PCs. (b) On the first day of wound healing, the number of PCs increased significantly, but both PCs and endothelial cells were disorganized. (c) On day 3 of wound healing, the lumen-like structures of vessels gradually formed. (d) On day 5 of wound healing, the lumen of vessels wrapped by pericytes was in good shape, but the vessels containing only endothelial cells had difficulty forming lumen-like structures. (e) On day 7 of wound healing, the vessels without PCs gradually degenerated and disappeared, and the intact vessels with PCs were observed. (f) The ratio of pericyte/endothelial cells was analyzed in a rat skin wound model by calculating the ratio of green/red immunofluorescence area. N = 12. (g) The normal skin (right side of the white line) and new wound-healing tissues (left side of the white line) were observed using immunofluorescence staining. Scale bar = 100 μm.

our study, we detected a high positive expression level of α-SMA and a low ratio of PCs to endothelial cells in the skin. These different results may be related to different functions of various tissues, which indicates that PCs have tissue specificity.

It has been reported that PCs in the cerebral vasculature and retina usually exhibit a reticular or stellate structure with multiple contacts and display a round structure in the kidney [34]. In this work, human skin PCs harbored a structure of double protrusions, with thin and long cell

protrusions extending on both sides of the skin PCs. This demonstrates that the morphological structure and number of PCs vary in different tissues.

Angiogenesis is critical for wound healing. Vessels act as channels for the transportation of nutrients and water, and the luminal structure of vessels serves as the foundation for their function. According to prior studies, human brain vascular PCs do not migrate and proliferate under serum-free conditions in 3D matrices [12,39]. But the coculture of PCs with human umbilical vein endothelial cells (HUVECs) promotes the activity of PCs, indicating that PCs are elongated and recruited to the surface of HUVECs [40]. Herein, HDMECs were arranged in a cobblestone-like shape and failed to form a lumen in 2D. HDMECs only formed lumen-like structures in a 3D environment, which could not last longer than 24 hours. In contrast, skin PCs could form lumen-like structures in both 2D and 3D environments, which differed from the previously reported characterization of PCs. This may be attributed to the different sources of PCs, indicating that PCs have tissue specificity. Previous studies have mostly focused on cerebrovascular PCs [41,42], and we concentrated on the tube-forming ability of skin PCs in this study.

Interestingly, we discovered that hypoxia or starvation could induce PCs to form lumen-like structures in a 2D culture environment. If not induced, about 40% of the PCs had difficulty forming lumen-like structures in our study. Hypoxia has been shown to promote PC proliferation and differentiation by stimulating the production of cytokines such as hypoxia-inducible factor-1 (HIF-1) [43]. The explanation for this may be that hypoxia promotes the tube formation of PCs. To our knowledge, no endothelial cells have been documented to have such a function. Limited reports of pluripotent stem cells that could form lumens have been documented [44], and no differentiated cells have exhibited such a function. An earlier study found that PCs promote skin regeneration by inducing epidermal cell polarity [15]. Our study concluded that PCs may promote skin regeneration by facilitating vascular lumen formation.

The relationships between endothelial cells and PCs have been the subject of certain investigations. For example, it has been reported that endothelial cells can recruit PCs, which promotes vascular maturation and maintains vascular stability [39]. Platelet-derived growth factor-B (PDGF-B), endothelin-1 (ET-1), transforming growth factor-β (TGF-β), heparin-binding epidermal growth factor (HB-EGF), and other chemotactic regulators are involved in this recruitment [12,40,45]. In this study, we revealed the mutual chemotaxis between HDMECs and skin PCs. This further expands our understanding of the interactions between PCs and endothelial cells.

PCs have been shown to aid in wound healing by reducing the recruitment of inflammatory cells and collagen deposition while promoting wound closure and tissue repair [46]. Our investigation yielded similar results. We found that PCs contributed to the formation of lumen-like structures in the rat model of skin wounds, which is beneficial for wound healing.

Furthermore, we found that the balance between PCs and endothelial cells is important for wound repair. A significant rise in the number of PCs was observed during the early stage of wound angiogenesis, and only vascular structures containing both PCs and endothelial cells stably existed during the late stage. We also noticed that the ratio of pericyte/endothelial cells began to decline on day 5 of wound healing. This may result from the fact that some cells can secrete vascular endothelial growth factor (VEGF) during wound healing [47,48], which gradually leads to the proliferation of endothelial cells. However, the ratio of pericyte/endothelial cells appeared to increase on day 7. It might be argued that the lack of nutritional assistance caused the eventual deterioration of the endothelial cells that make up the vascular structures. In order to promote wound healing, the pericyte/endothelial cell ratio should be balanced. To sum up, this study described the structure and function of skin PCs and clarified the important role of PCs during skin wound healing and angiogenesis. It is the first study to demonstrate that skin PCs have excellent tube formation capability and chemotactic effect on endothelial cells. However, there are still some limitations in this study. For instance, there is no direct evidence that skin PCs can guide angiogenesis. Therefore, further exploration and analysis through *in vivo* imaging or other technologies are required. The direct role of PCs in wound repair has not been fully studied, either. In addition, it is necessary to investigate the mechanism of mutual chemotaxis between PCs and endothelial cells and determine whether any related chemokines are involved.

Conclusions

In summary, skin PCs have a special structure of double protrusions and excellent tube-forming capability. PCs could form lumen-like structures in 2D and matrigel. Furthermore, skin PCs have chemotaxis to endothelial cells and can recruit endothelial cells to accelerate the formation of lumen-like structures. The wound repair may benefit from balancing the pericyte/endothelial cell ratio in rat models of skin wounds. PCs might promote wound repair by recruiting endothelial cells.

Abbreviations

2D, two dimensional; 3D, three dimensional; BSA, bovine serum albumin; DMEM, dulbecco's modified eagle medium; ECM, endothelial cell medium; ET-1, endothelin-1; FBS, fetal bovine serum; FB, fibroblast; HDMECs, human dermal microvascular endothelial cells; HIF-1, hypoxia-inducible factor-1; HUVEC, human umbilical vein endothelial cells; NG2, neural/glial antigen 2; PBS, phosphate-buffered saline; PCs, pericytes; PDGF-

B, platelet-derived growth factor-B; PDGFR-β, platelet-derived growth factor receptor-β; PGF, pericyte growth factor; TGF-β, transforming growth factor-β; VEGF, vascular endothelial growth factor; α-SMA, alpha-smooth muscle actin.

Availability of Data and Materials

The data used to support the findings of this study are available from the corresponding author upon request.

Author Contributions

YC and HL conceptualized and designed the study, and drafted the initial manuscript. YZ and JM performed the research. JL analyzed the data. All authors contributed to editorial changes in the manuscript. All authors read and approved the final manuscript. All authors approved the final manuscript as submitted and agreed to be accountable for all aspects of the work.

Ethics Approval and Consent to Participate

This study was approved by the Ethics Committee of Anzhen Hospital (Approval number: 2023087x), and all patients have signed informed consent forms. All procedures were conducted in accordance with approved guidelines and the ethical requirements of the Helsinki Declaration. All procedures of animal trials were carried out in accordance with the National Institutes of Health Guide for the Care and Use of Laboratory Animals and the animal protocols were approved by the Ethics Committee of the Institute of Zoology Chinese Academy of Sciences (IOZ-IACUC-2023-007).

Acknowledgment

Not applicable.

Funding

Our research was supported by the National Natural Science Foundation of China (No.81971849) and the Natural Science Foundation of Beijing Municipality (No.7212026).

Conflict of Interest

The authors declare no conflict of interest.

Supplementary Material

Supplementary material associated with this article can be found, in the online version, at https://doi.org/10.24976/Discov.Med.202436181.29.

References

[1] Orekhov AN, Bobryshev YV, Chistiakov DA. The complexity of cell composition of the intima of large arteries: focus on pericyte-like cells. Cardiovascular Research. 2014; 103: 438–451.

[2] Uusitalo-Kylmälä L, Joensuu K, Hietanen K, Paloneva J, Heino TJ. Evidence for the in vivo existence and mobilisation of myeloid angiogenic cells and pericyte-like cells in wound patients after skin grafting. Wound Repair and Regeneration. 2023; 31: 111–119.

[3] Burdyga T, Borysova L. Calcium signalling in pericytes. Journal of Vascular Research. 2014; 51: 190–199.

[4] Nourshargh S, Alon R. Leukocyte migration into inflamed tissues. Immunity. 2014; 41: 694–707.

[5] Birbrair A, Zhang T, Wang ZM, Messi ML, Mintz A, Delbono O. Pericytes at the intersection between tissue regeneration and pathology. Clinical Science. 2015; 128: 81–93.

[6] Paquet-Fifield S, Schlüter H, Li A, Aitken T, Gangatirkar P, Blashki D, *et al*. A role for pericytes as microenvironmental regulators of human skin tissue regeneration. The Journal of Clinical Investigation. 2009; 119: 2795–2806.

[7] Zhuang L, Visalakshan RM, Kaur P. Dermal Pericytes Exhibit Declined Ability to Promote Human Skin Regeneration with Ageing in 3D Organotypic Culture Models. Cells. 2021; 10: 3051.

[8] Evdokiou A, Kanisicak O, Gierek S, Barry A, Ivey MJ, Zhang X, *et al*. Characterization of Burn Eschar Pericytes. Journal of Clinical Medicine. 2020; 9: 606.

[9] Meijer EM, van Dijk CGM, Kramann R, Verhaar MC, Cheng C. Implementation of Pericytes in Vascular Regeneration Strategies. Tissue Engineering. Part B, Reviews. 2022; 28: 1–21.

[10] Laurenzana A, Fibbi G, Margheri F, Biagioni A, Luciani C, Del Rosso M, *et al*. Endothelial Progenitor Cells in Sprouting Angiogenesis: Proteases Pave the Way. Current Molecular Medicine. 2015; 15: 606–620.

[11] Blanco R, Gerhardt H. VEGF and Notch in tip and stalk cell selection. Cold Spring Harbor Perspectives in Medicine. 2013; 3: a006569.

[12] Kemp SS, Aguera KN, Cha B, Davis GE. Defining Endothelial Cell-Derived Factors That Promote Pericyte Recruitment and Capillary Network Assembly. Arteriosclerosis, Thrombosis, and Vascular Biology. 2020; 40: 2632–2648.

[13] Lindblom P, Gerhardt H, Liebner S, Abramsson A, Enge M, Hellstrom M, *et al*. Endothelial PDGF-B retention is required for proper investment of pericytes in the microvessel wall. Genes & Development. 2003; 17: 1835–1840.

[14] Yuge S, Ishii T, Noishiki C, Fukuhara S. Novel regulatory mechanisms underlying angiogenesis during wound healing revealed by fluorescence-based live-imaging in zebrafish. Journal of Biochemistry. 2023; 174: 5–12.

[15] Zhuang L, Lawlor KT, Schlueter H, Pieterse Z, Yu Y, Kaur P. Pericytes promote skin regeneration by inducing epidermal cell polarity and planar cell divisions. Life Science Alliance. 2018; 1: e201700009.

[16] Morikawa S, Iribar H, Gutiérrez-Rivera A, Ezaki T, Izeta A. Pericytes in Cutaneous Wound Healing. Advances in Experimental Medicine and Biology. 2019; 1147: 1–63.

[17] Bodnar RJ, Satish L, Yates CC, Wells A. Pericytes: A newly recognized player in wound healing. Wound Repair and Regeneration. 2016; 24: 204–214.

[18] Thomas H, Cowin AJ, Mills SJ. The Importance of Pericytes in Healing: Wounds and other Pathologies. International Journal of Molecular Sciences. 2017; 18: 1129.

[19] Cai W, Liu H, Zhao J, Chen LY, Chen J, Lu Z, *et al*. Pericytes in Brain Injury and Repair After Ischemic Stroke. Translational

Stroke Research. 2017; 8: 107–121.
[20] Das S, Baker AB. Biomaterials and Nanotherapeutics for Enhancing Skin Wound Healing. Frontiers in Bioengineering and Biotechnology. 2016; 4: 82.
[21] Veith AP, Henderson K, Spencer A, Sligar AD, Baker AB. Therapeutic strategies for enhancing angiogenesis in wound healing. Advanced Drug Delivery Reviews. 2019; 146: 97–125.
[22] Morbidelli L, Genah S, Cialdai F. Effect of Microgravity on Endothelial Cell Function, Angiogenesis, and Vessel Remodeling During Wound Healing. Frontiers in Bioengineering and Biotechnology. 2021; 9: 720091.
[23] Zhao Y, Ma J, Cui Y, Lin H. A method to isolate human dermal microvascular pericytes without the use of magnetic beads sorting in vitro. Tissue & Cell. 2023; 84: 102171.
[24] Lu K, Wang Y, Wang H, Guan X, Wang L, Xin Y, *et al*. Primary cultured and establishment of hypoxic/reoxygenation model of human dermal microvascularendothelial cells. Journal of Cardiovascular and Pulmonary Diseases. 2015; 34: 132–136. (In Chinese)
[25] Williams R, Thornton MJ. Isolation of Different Dermal Fibroblast Populations from the Skin and the Hair Follicle. Methods in Molecular Biology. 2020; 2154: 13–22.
[26] Crisan M, Corselli M, Chen WCW, Péault B. Perivascular cells for regenerative medicine. Journal of Cellular and Molecular Medicine. 2012; 16: 2851–2860.
[27] Hou H, Li J, Zhou L, Liang J, Wang J, Li J, *et al*. An effective method of isolating microvascular endothelial cells from the human dermis. Cell Biology International. 2020; 44: 2588–2597.
[28] Song J, Zhang Y, Pan H, Xu X, Deng CC, Yang B. Isolation, Culture, and Characterization of Primary Dermal Fibroblasts from Human Keloid Tissue. Journal of Visualized Experiments. 2023; 197: e65153.
[29] Kelley M, Fierstein S, Purkey L, DeCicco-Skinner K. Endothelial Cell Tube Formation Assay: An In Vitro Model for Angiogenesis. Methods in Molecular Biology. 2022; 2475: 187–196.
[30] Rumianek AN, Greaves DR. How Have Leukocyte In Vitro Chemotaxis Assays Shaped Our Ideas about Macrophage Migration? Biology. 2020; 9: 439.
[31] Bourland J, Mayrand D, Tremblay N, Moulin VJ, Fradette J, Auger FA. Isolation and Culture of Human Dermal Microvascular Endothelial Cells. Methods in Molecular Biology. 2019; 1993: 79–90.
[32] Kondo T, Hosoya KI, Hori S, Tomi M, Ohtsuki S, Takanaga H, *et al*. Establishment of conditionally immortalized rat retinal pericyte cell lines (TR-rPCT) and their application in a co-culture system using retinal capillary endothelial cell line (TR-iBRB2). Cell Structure and Function. 2003; 28: 145–153.
[33] Hartmann DA, Coelho-Santos V, Shih AY. Pericyte Control of Blood Flow Across Microvascular Zones in the Central Nervous System. Annual Review of Physiology. 2022; 84: 331–354.
[34] Caporarello N, D'Angeli F, Cambria MT, Candido S, Giallongo C, Salmeri M, *et al*. Pericytes in Microvessels: From "Mural" Function to Brain and Retina Regeneration. International Journal of Molecular Sciences. 2019; 20: 6351.
[35] Armulik A, Genové G, Mäe M, Nisancioglu MH, Wallgard E, Niaudet C, *et al*. Pericytes regulate the blood-brain barrier. Nature. 2010; 468: 557–561.
[36] Zhao Z, Nelson AR, Betsholtz C, Zlokovic BV. Establishment and Dysfunction of the Blood-Brain Barrier. Cell. 2015; 163: 1064–1078.
[37] Caporali A, Martello A, Miscianinov V, Maselli D, Vono R, Spinetti G. Contribution of pericyte paracrine regulation of the endothelium to angiogenesis. Pharmacology & Therapeutics. 2017; 171: 56–64.
[38] Erdener ŞE, Küreli G, Dalkara T. Contractile apparatus in CNS capillary pericytes. Neurophotonics. 2022; 9: 021904.
[39] Stratman AN, Schwindt AE, Malotte KM, Davis GE. Endothelial-derived PDGF-BB and HB-EGF coordinately regulate pericyte recruitment during vasculogenic tube assembly and stabilization. Blood. 2010; 116: 4720–4730.
[40] Kemp SS, Lin PK, Sun Z, Castaño MA, Yrigoin K, Penn MR, *et al*. Molecular basis for pericyte-induced capillary tube network assembly and maturation. Frontiers in Cell and Developmental Biology. 2022; 10: 943533.
[41] Whitehead B, Karelina K, Weil ZM. Pericyte dysfunction is a key mediator of the risk of cerebral ischemia. Journal of Neuroscience Research. 2023; 101: 1840–1848.
[42] Brown LS, Foster CG, Courtney JM, King NE, Howells DW, Sutherland BA. Pericytes and Neurovascular Function in the Healthy and Diseased Brain. Frontiers in Cellular Neuroscience. 2019; 13: 282.
[43] Wen J, Wang D, Cheng L, Wu D, Qiu L, Li M, *et al*. The optimization conditions of establishing an H9c2 cardiomyocyte hypoxia/reoxygenation injury model based on an AnaeroPack System. Cell Biology International. 2021; 45: 757–765.
[44] Taniguchi K, Shao Y, Townshend RF, Tsai YH, DeLong CJ, Lopez SA, *et al*. Lumen Formation Is an Intrinsic Property of Isolated Human Pluripotent Stem Cells. Stem Cell Reports. 2015; 5: 954–962.
[45] Bhowmick S, D'Mello V, Caruso D, Wallerstein A, Abdul-Muneer PM. Impairment of pericyte-endothelium crosstalk leads to blood-brain barrier dysfunction following traumatic brain injury. Experimental Neurology. 2019; 317: 260–270.
[46] Bodnar RJ, Yang T, Rigatti LH, Liu F, Evdokiou A, Kathju S, *et al*. Pericytes reduce inflammation and collagen deposition in acute wounds. Cytotherapy. 2018; 20: 1046–1060.
[47] Takahashi H, Shibuya M. The vascular endothelial growth factor (VEGF)/VEGF receptor system and its role under physiological and pathological conditions. Clinical Science. 2005; 109: 227–241.
[48] Aguilera KY, Brekken RA. Recruitment and retention: factors that affect pericyte migration. Cellular and Molecular Life Sciences. 2014; 71: 299–309.